# Stabilization of an InP mode-locked laser PIC through simultaneous optical filtering and self-injection locking using a Fabry-Perot etalon

Srinivas Varma Pericherla, Lawrence Trask, Chinmay Shirpurkar, Graduate Student Member, IEEE, Ashish Bhardwaj, Gloria E. Hoefler, Peter J. Delfyett, *Fellow, IEEE* 

Abstract—We report experimental studies of a self-injection locking technique with optically filtered feedback and its influence on optical linewidth, RF linewidth, carrier side-band suppression and frequency stability of a monolithically integrated InP passive mode-locked laser. We use a Fabry-Perot etalon as the photonic filter placed in an external fiber feedback loop for filtering the mode-locked laser output and subsequently self-injection locking. Using this technique, we demonstrate optical axial mode linewidth narrowing by a factor of 100x from 600 MHz to 6 MHz, while improving the RF linewidth by a factor of 50x from 109 kHz to 2.2 kHz. The external cavity modes arising from the fiber feedback loop were suppressed by 20 dB, while the phase noise at 200 kHz offset from the carrier is suppressed by 35 dB. Finally, we implement a coupled optoelectronic loop by using the photo-detected output from the self-injection locked laser and provide feedback to drive the integrated electro-absorption modulator in the laser cavity. The coupled optoelectronic loop is referenced to an external RF source to transfer the stability and further improve the noise performance of the self-injection locked laser. The Allan deviation at 10 s averaging time is 5 x 10<sup>-12</sup>, showing an improvement of 5 orders of magnitude over passive mode-locking operation.

Index Terms—Semiconductor mode-locked laser, photonic integrated circuit, injection locking, coupled opto-electronic loop.

### I. INTRODUCTION

EMICONDUCTOR mode-locked lasers are a compact and versatile optical frequency comb sources. Optical frequency combs are critical for a wide range of applications such as laser ranging [1], high-speed optical interconnects [2], frequency synthesis, spectroscopy and photonic signal processing [3], [4]. Semiconductor mode-locked lasers (MLL) are capable of generating widely spaced frequency combs ranging from a GHz to few 10's of GHz, with potential for wide ranging applications such as telecommunications [5], optical frequency division and low-noise microwave signal generation [6], [7]. Chip-scale integrated MLL's based on

This work was supported in part by the NSF IUCRC 2052701 (Corresponding author: Srinivas Varma Pericherla).

Srinivas Varma Pericherla and Peter J. Delfyett are with College of Optics and Photonics, University of Central Florida, Orlando, FL 32816 USA and also Department of Electrical Engineering, University of Central Florida, Orlando, FL 32816 USA (e-mail: srinivasvarma.pericherla@ucf.edu; delfyett@creol.ucf.edu).

Peter J. Delfyett is also with Department of Physics , University of Central Florida, Orlando, FL 32816 USA.

Chinmay Shirpurkar and Lawrence Trask are with College of Optics and Photonics, University of Central Florida, Orlando, FL 32816 USA.

Ashish Bharadwaj and Gloria E. Hoefler are with Infinera corporation, Sunnyvale, CA 9408 USA.

Manuscript received December 15, 2022; revised April 16, 2023.

CMOS compatible material platforms such as InP, InP on silicon and InGaAs/AlGaAs on silicon have been demonstrated in the past [8] offering high volume manufacturing capability. In addition, semiconductor MLL's also offer high efficiency, ease of operation and access to a myriad of wavelengths.

Most of the applications benefit from the comb sources with widely spaced optical modes with narrow optical linewidth and good frep stability. However, semiconductor monolithic MLL's with comb spacing of 10's of GHZ often produce axial mode linewidths on the order of 10's - 100's of MHz due to waveguide losses, frequency noise/jitter and gain saturation among other factors [9]. Multiple techniques have been demonstrated in the past improving the performance of the chip-scale MLL's. One of these techniques employ an external fiber loop feedback (loop length - 120 m) and a narrow linewidth CW laser for injection locking to suppress instabilities and reduce the phase noise closer to the carrier, resulting in RF linewidth narrowing from 100 kHz to 1 kHz [10]. Although the noise performance closer to the carrier improved, the supermodes from external fiber feedback loop remain unsuppressed and no optical linewidth improvement was reported. Another approach that uses a coupled optoelectronic oscillator (COEO) technique and an external narrow linewidth CW laser for injection locking has been demonstrated [11], showing improvements in frep stability, RF and optical linewidth. However, the cavity modes from the COEO loop persists and noise reduction was only observed within 3-5 dB from the peak of the optical mode while rest of the noise remain unsuppressed. Our technique improves upon previous demonstrations [10], [11], by simultaneously suppressing the feedback cavity supermodes and improving the optical axial mode linewidth with higher noise suppression.

In this paper we report an injection locking technique using a Fabry-Perot Etalon (FPE) as a photonic filter in conjunction with an external fiber loop feedback for self-injection locking the MLL. This paper is organized as follows: In section II, we introduce the concepts of injection locking, influence of optical/RF filtering and feedback. We discuss about the monolithic MLL PIC source and FPE used in the experiment. In section III, we discuss the improvements in RF, optical linewidth,  $f_{rep}$  stability and supermode noise suppression due to the optical filtering and self-injection locking. In section IV, we discuss the implementation of a coupled opto-electronic loop (COEL) referenced to an external RF source, to further improve the phase noise and  $f_{rep}$  stability of the MLL.

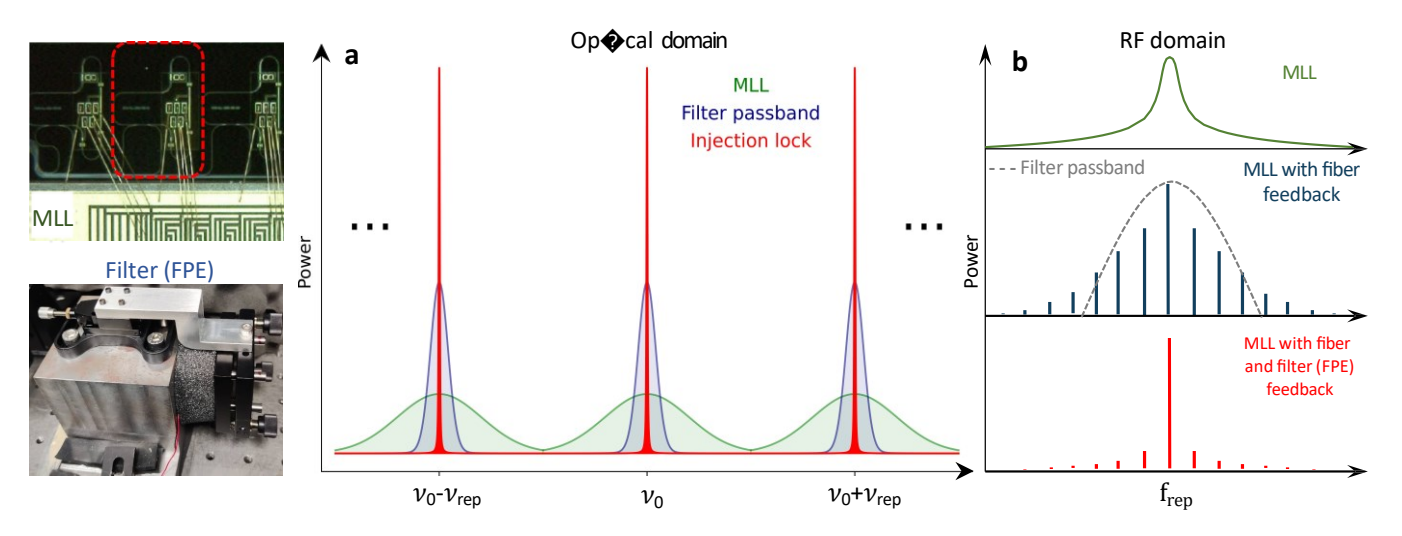


Fig. 1. Images showing the monolithic Indium Phosphide (InP) mode-locked laser source and Fabry-Perot Etalon (photonic filter) used in the experiment. (a) Concept mode-locked laser frequency noise and linewidth reduction due to self-injection locking. Plot shows the optical mode linewidth of the MLL under passive mode-locking operation (green), Etalon resonance passband (blue) and reduced linewidth of the laser when self-injection locked (red). (b) Concept enhancement of the RF power spectrum of the MLL  $f_{rep}$  signal (green) when injection locked with feedback from fiber loop (blue) resulting in supermode noise and feedback from fiber loop with a photonic filter (red) showing supermode noise suppression.

#### II. FUNDAMENTAL CONCEPTS, MLL AND FPE

#### A. Linewidth broadening and self-injection locking

The laser linewidth broadening typically comes from phase fluctuations of the optical field, which comes from the fluctuations due to spontaneous emission events [12]. In addition to the phase noise, the noise resulting from spontaneous emission events also induces fluctuation in photon numbers leading to amplitude noise. This amplitude noise causes fluctuations in carrier density thereby changing the refractive index of the material resulting in frequency noise. Additionally, in semiconductor mode-locked lasers, the pulse interaction causes changes in carrier density leading to a change in refractive index, causing a spectral shift to longer wavelengths, thus resulting in broadening of the optical modes [13]. The linewidth broadening and chirp due to fluctuations in carrier density can be characterized by linewidth enhancement factor (a - parameter) and this can vary over the wavelength range [14]. In passive MLL's the timing jitter of the pulses also results in additional linewidth broadening which depends on the square of the mode number therefore the wavelength [15]. This could result in the linewidth of the passive MLL comb to resemble a parabolic function which is a function of mode number/wavelength. Further, the minimum linewidth can be shifted from the center of the MLL spectrum due to the chirp of the pulses circulating the cavity [14].

Self-injection of lasers coupled to a high-Q resonator is a powerful technique and it can lead to stabilization of the laser frequency and significant linewidth reduction. Injection locking process occurs when the laser frequency gets closer to a resonance of the high-Q resonator within the locking bandwidth of the laser. The injection locking bandwidth depends on parameters such as the cavity dispersion and feedback strength. Self-injection locking in CW lasers has been demonstrated in the past using whispering gallery mode resonator (WGMR) [16] and high Q F-P resonator [17] achieving narrow linewidths. While these demonstrations mainly focus on single

mode CW lasers, this technique can be extended and used for MLL combs comprising of several optical axial modes each separated by  $f_{rep}$ .

Multi-tone injection locking technique [6] has been demonstrated in the past, where multiple axial modes from an external comb source are injected into an MLL, where the MLL frep is close to a sub-harmonic of the injected comb's repetition rate. Similarly, to implement self-injection locking in an MLL coupled to a high Q photonic filter, the  $f_{rep}$  of the MLL has to be matched with the FSR of the filter and the MLL should also have the capability to tune the comb frequency independent of the  $f_{rep}$ . Fig. 1a shows the depiction of the optical axial modes of the MLL under injection locking operation. The plot in green shows the optical axial modes of the MLL under passive mode-locking (PML) operation, blue shows the resonance peaks of a photonic filter with a passband narrower that the linewidth of the MLL comblines and color red shows the optical axial modes when the MLL is operating in self-injection locked regime. Fig. 1b shows the conceptual RF power spectrum of the  $f_{rep}$  signal when the MLL is under PML operation (green) and RF power spectrum when the MLL is self-injection locked with feedback from an external fiber loop (blue) showing the supermodes resulting from the fiber loop. The depiction of the RF power spectrum (red) when the laser is injection locked with feedback from fiber with a photonic filter placed in the loop shows suppression of the supermodes arising from the fiber loop. It should be noted that the fiber feedback alone improves the noise closer to the carrier while introducing supermode noise at farther offsets. The photonic filter here helps to suppress the supermode noise, in addition to improving the noise closer to the carrier.

### B. Monolithic InP MLL and FPE

We used a monolithically integrated Indium Phosphide (InP) based MLL [18] depicted in the schematic in Fig. 2. The MLL cavity is implemented by using a gain section, saturable ab-

sorber (SA), electro-absorption modulator (EAM) and a multimode interference (MMI) coupler in a racetrack configuration. The MLL cavity length is defined lithographically, to operate the laser at a fundamental  $f_{rep} \sim 10$  GHz. The MLL operates in a colliding pulse operation where two pulses counterpropagate in the cavity. The gain section in the cavity is 1mm long and placed in between the SA and EAM sections. The SA (length ~60 µm) and EAM sections are separated by half the cavity length to ensure collision of the counter propagating pulses in both SA and EAM sections. This approach offers an advantage by providing equal time for the gain to recover from the carrier depletion, caused by each pulse propagating through the gain section. The EAM section is designed to provide 10 dB extinction, which can be used for independent active loss modulation to enable hybrid mode-locking without changing the reverse bias of the SA section.

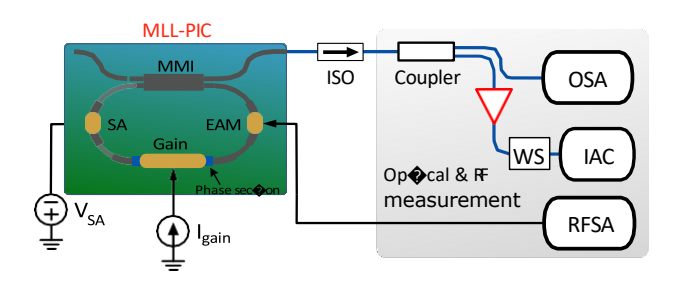


Fig. 2. Schematic of the InP mode-locked laser showing the cavity elements and diagnostics. EAM: Electro-absorption modulator, SA: Saturable absorber, OSA: Optical spectrum analyzer, WS: Waveshaper, IAC: Intensity Autocorrelator, RFSA: RF spectrum analyzer

The MLL operates at an  $f_{rep} \sim 10$  GHz and can be tuned over 50 MHz by changing the bias conditions of the gain and SA sections. The MLL cavity also consists of a thermally tuned integrated phase section to enable cavity mode tuning ( $f_{ceo}$ ) independent of the MLL  $f_{rep}$ . The EAM section can also be used as a photodetector to monitor the  $f_{rep}$  signal of the MLL. The integrated 2 x 2 MMI coupler in the cavity acts as an output coupler with a 80/20 coupling ratio. An average power of  $\sim 150~\mu{\rm W}$  is coupled out using a tapered fiber.

Optical spectrum of the MLL under PML operation is shown in Fig. 3a. Fig. 3b shows the optical axial mode linewidth one of the comb component near the center of the optical spectrum measured via optical heterodyne beat measurement technique using a narrow linewidth tunable CW laser. The RF spectrum of the amplified  $f_{rep}$  signal from the integrated EAM section, when the MLL is under PML operation is plotted in Fig. 3c. Fig. 3d shows the phase section response where plot shows the variation of comb frequency  $(\Delta v)$  and repetition rate  $(\Delta f_{rep})$  when the phase section bias current  $I_{phase}$  is varied. It should be noted that the relative change in  $\Delta v$  is higher compared to the  $\Delta f_{rep}$  and we use this feature in the experiments to shift the comb frequency while keeping the  $f_{rep}$  relatively unchanged.

The FPE used for optical filtering consists of two Planoconcave mirrors, having a radius of curvature (ROC) of 1 m. The mirrors are separated by 15 mm (air space), so that the free spectral range (FSR) of the FPE modes matches with the MLL's  $f_{rep}$ . We measured the FPE resonance width to be

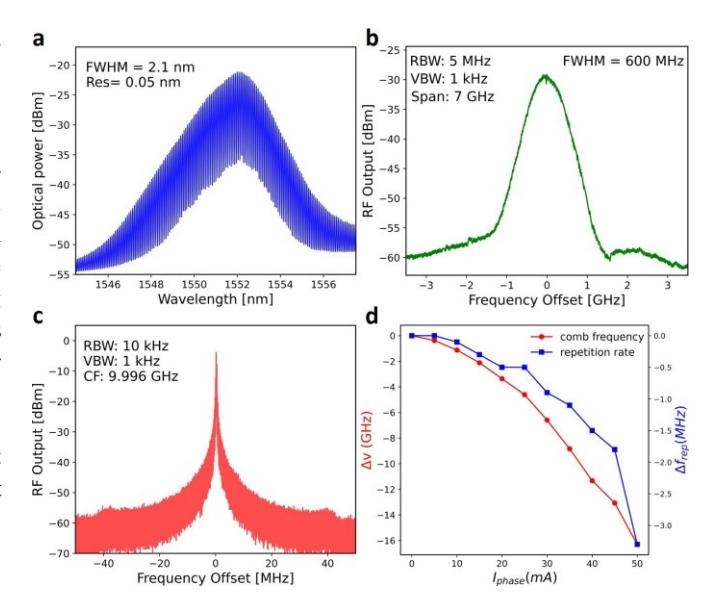


Fig. 3. (a) The optical spectrum of the MLL under PML operation, (b) measured optical axial mode linewidth of the MLL under PML operation via optical heterodyne detection technique, (c) RF spectrum of the MLL  $f_{rep}$  signal under PML operation, CF: center frequency (d) phase section response to the applied bias, plot shows variation of comb frequency ( $\Delta v$ ) and repetition rate ( $\Delta f_{rep}$ ) with changing bias current

49 MHz, by passing ASE from an EDFA through the FPE and photodetecting the beat note from the output signal. The mirrors are held in place by COTS mirror mounts anchored to a steel block for stability. An image of the FPE is shown in Fig. 1. Additional acoustic and thermal isolation is provided by placing the FPE in a temperature controlled box with resistive heaters and isolation foam. One of the mirror mounts is attached to a tunable stage that is anchored to the steel block to offer the coarse tunability required for matching the FSR of the FPE to the MLL's  $f_{rep}$ .

## III. SELF-INJECTION THROUGH FILTERED OPTICAL FEEDBACK

In this section we will discuss the optical filtering and selfinjection locking process of the MLL with the FPE in the fiber feedback loop as depicted in Fig. 4. First the MLL is operated in PML operation by applying bias to the gain and SA sections. The coupled output from the MLL is passed through the circulator to avoid any back reflections and injected into a fiber coupled semiconductor optical amplifier (SOA) to amplify the signal from -10 dBm to 8 dBm. Amplified output from the SOA is sent through the FPE to filter the optical axial modes of the MLL. The light is coupled in and out of the FPE using a pair of achromatic focusers with a beam waist of 420 µm that closely matches the waist of the FPE, considering the mirror ROC of 1m. Insertion loss due to coupling in and out of the FPE is 4 dB. The filtered output from the FPE is passed through 20:80 coupler which keeps 20 % of the light in the loop which is then passed through a variable optical delay (VOD) and variable optical attenuator (VOA). Typically 150  $\mu$ W of average power is injected back into the MLL via the tapered fiber located after the circulator. After the coupling

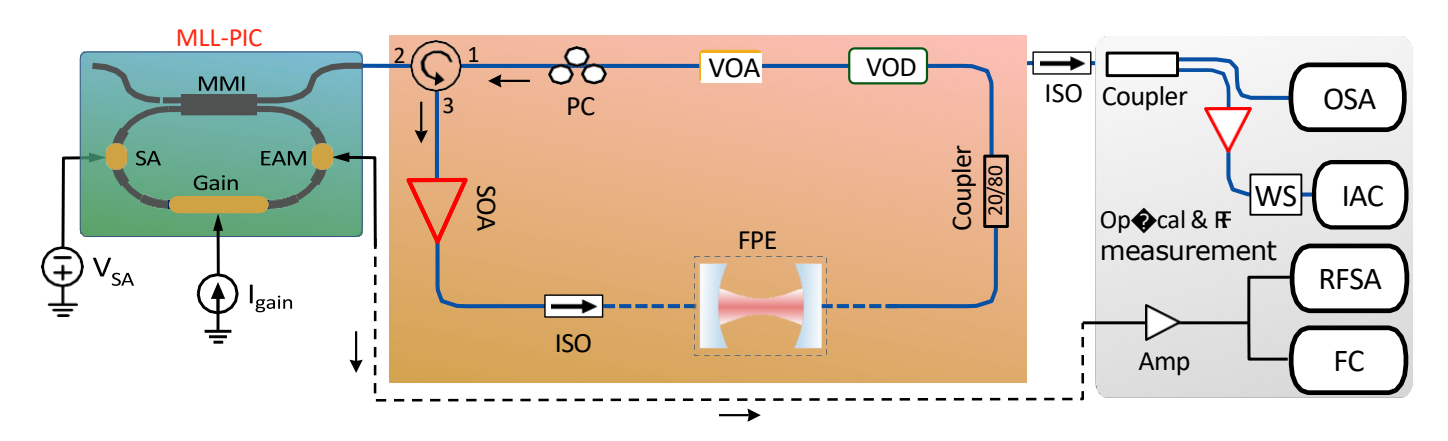


Fig. 4. Schematic of the monolithic InP MLL, optical filtering and injection locking apparatus used in the experiment. EAM: Electro-absorption modulator, MMI: Multi-mode interference coupler, SOA: Semiconductor laser amplifier, SA: saturable absorber, FPE: Fabry-Perot etalon, VOD: Variable optical delay, VOA: Variable optical attenuator, ISO: Isolator, Amp: RF amplifier, OSA: Optical spectrum analyzer, WS: Waveshaper, IAC: Intensity auto-correlator, RFSA: RF spectrum analyzer, FC: Frequency counter

losses and MMI coupler, 10 - 15  $\mu$ W of injected power gets coupled into the MLL cavity which ensured stable operation in our experiments.

For the injection locking process to occur, all three cavity modes i.e., MLL, fiber feedback loop and the FPE must be overlapped. This is done by matching the  $f_{rep}$  of the MLL to the FSR of the FPE which is 9.996 GHz, by varying the bias conditions of the gain and SA sections. After the  $f_{rep}$  is matched, the integrated phase section bias is varied to shift the comb frequency (i.e, frequency of the optical modes), without affecting the  $f_{rep}$ . When the axial modes of the MLL match with the FPE resonances, sufficient amount of light passes through the FPE to initiate the self-injection locking process. The variable optical delay in the fiber feedback loop is varied to align the fiber cavity modes with that of the FPE and MLL, leading to further optimization of the self-injection locking.

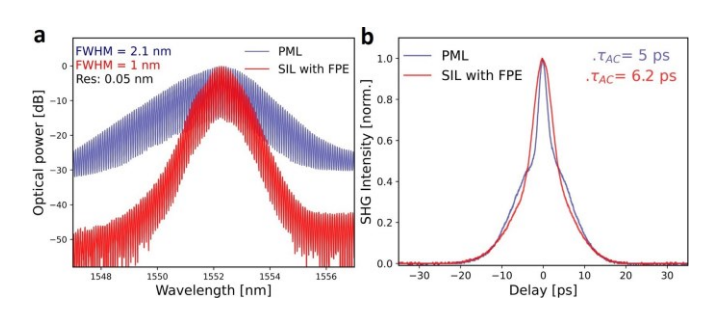


Fig. 5. (a) Optical spectrum of the MLL under PML (blue) and self-injection locking (SIL) with filtered feedback (red), (b) measured intensity autocorrelation of the compressed pulse under PML operation (blue) and compressed output pulse under SIL operation with filtered feedback (red)

The optical spectrum of the MLL under self-injection locking (SIL) with filtered feedback and PML operation is shown in Fig. 5a. The optical spectrum of the MLL under SIL operation with the FPE as the photonic filter is noticeably narrower, in comparison with the PML operation. One possible explanation could be the optical axial mode walk-off from the center frequency between the MLL and the FPE due to dispersion mismatch. It should be noted that we have observed that the transmission optical spectra of the MLL through the FPE without injection locking looks similar to the optical

spectrum of the MLL under SIL with FPE operation. The pulses coming out of the MLL under PML operation are upchirped and 12.5 ps in duration. We use a programmable waveshaper to compress the pulses by only compensating for the linear chirp, thereby compressing the pulses to 5 ps as shown in Fig. 5b, which is 3.3 times the transform-limited pulse duration, indicating residual high-order chirp. We

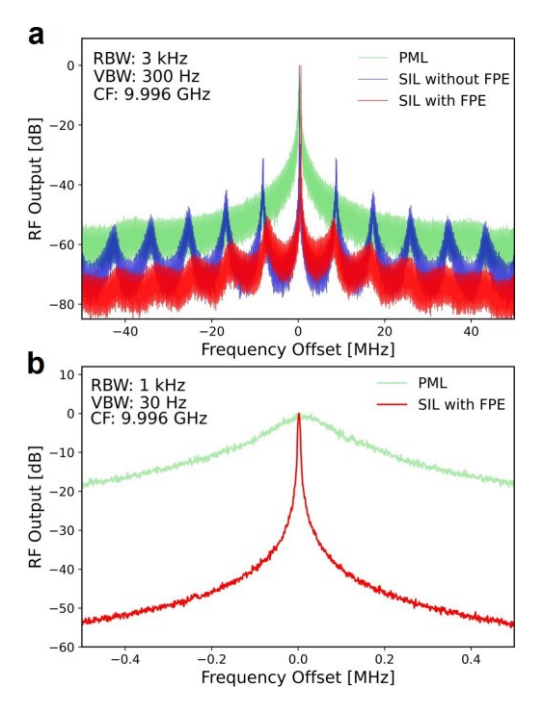


Fig. 6. RF spectrum of the  $f_{rep}$  signal from the integrated EAM, (a)  $f_{rep}$  signal of the MLL under PML, self-injection locking without the FPE in the fiber feedback loop (SIL without FPE) and self-injection locking with the FPE in the fiber feedback loop (SIL with FPE), CF: center frequency (b)  $f_{rep}$  signal of the MLL operating under PML and SIL with FPE at 1 MHz span

measure the pulses coming out of the laser under SIL operation to be 9 ps and up-chirped. These pulses are compressed to 6.2 ps which is 1.7 times the transform-limited pulse duration by compensating for the linear chirp. It can be observed that the pulses under SIL operation are compressed to a higher degree,

implying that linear chirp is dominant in this case, which can be expected as the self-injection locked lasers are are known to exhibit more linear chirp in some cases.

The RF spectra of the *frep* signal, with the MLL operating under PML, SIL without the FPE in the fiber feedback loop (SIL without FPE) and SIL with the FPE in the fiber feedback loop (SIL with FPE) is shown in Fig. 6a. The fiber cavity modes that are 8.21 MHz apart adjacent to the carrier (9.996 GHz) are suppressed by 20 dB, when the MLL is under SIL operation with the FPE filtering the optical axial modes. The supermode spurs separated by 8.21 MHz correspond to the external loop length of 19 meters which includes SMF 28 and FPE and another 2.5 meters of SMF 28 from the tapered fiber and optical circulator.

Fig. 6b shows the RF spectrum of the  $f_{rep}$  signal at 1 MHz span when the MLL is operating under PML and SIL with FPE filtering. The RF linewidth narrowed by a factor of 50 from 109 kHz to 2.2 kHz when the laser is operated in self-injection locking regime. The phase noise at 200 kHz offset from the carrier is suppressed by 35 dB when the MLL is under SIL with FPE operation. An RF linewidth of 2.01 kHz was observed with the MLL under SIL without FPE operation, which came at the cost of added supermode noise and no optical linewidth reduction.

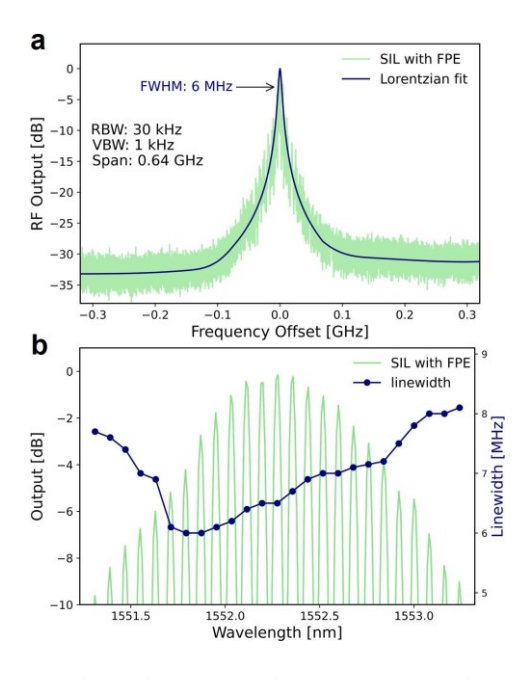


Fig. 7. Measured optical linewidth of the MLL operating under self-injection locking with filtered feedback (SIL with FPE) via optical heterodyne with narrow linewidth tunable CW laser, (a) RF spectrum of the measured optical axial mode linewidth with RBW: 30 kHz and VBW: 1kHz, (b) measured optical linewidth of all 25 comb-lines within 10 dB from the peak

We measure the optical linewidth of the MLL under PML and SIL with FPE operation, via optical heterodyne beat measurement with a narrow linewidth tunable CW laser (Agilent 81680A). Fig. 7a shows the measured beat signal of one of the MLL comb-lines demonstrating a FWHM of 6 MHz, when the MLL is operating under SIL with FPE. This demonstrates a significant reduction in optical axial-mode linewidth by factor of 100, from 600 MHz (Fig. 3d) to 6 MHz. The influence

of self-injection locking through filtered feedback on the comb-lines is studied by performing optical heterodyne beat measurement on all 25 comb-lines within 10 dB from the peak which is shown in Fig. 7b. The linewidth trend resembles an asymmetric parabolic shape which we attribute to the parabolic dependence of linewidth on the optical mode frequency [19] and the a - parameter [20].

We compare our experimental results with theoretical expectation, using the following equation [21] to estimate the optical linewidth, which considers the linewidth of the laser  $(\Delta \nu_o)$ , the a - parameter, power mode coupling factor  $\beta$ , finesse of the FPE  $(F_{FP})$ , finesse of the laser  $(F_l)$ , FPE cavity length  $(L_{FP})$  and laser cavity length  $(L_l)$ .

$$\Delta v = \frac{\Delta v_o}{[1 + (1 + a^2)^{1/2} \sqrt{\beta_{nl_t}^{LFP} F_{FP} \over Rl_t}]^2}$$
 (1)

 $\Delta v_o$  is measured to be 600 MHz, a is 4.5, the evaluated value of  $\beta$  is -15 dB,  $F_{FPE}$  is 200,  $F_l$  is 5,  $L_{FP}$  is 15 mm,  $L_l$  is 9.5 mm and n is 3.16. Considering these parameters, the estimated theoretical linewidth is 1.84 MHz, which is in close agreement with the measured linewidth. The small discrepancy between the theoretical and experimental linewidth could be due to error in considered parameters and noise contribution from external factors.

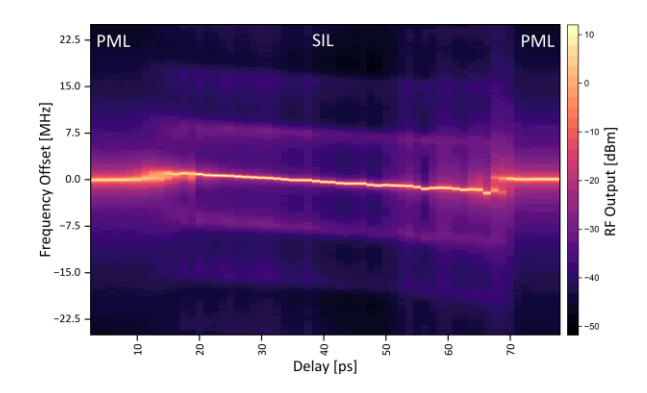


Fig. 8. Heatmap of the measured  $f_{rep}$  signal as the MLL goes through PML and SIL regimes, when the VOD in the fiber feedback path is varied. RBW: 10 kHz, VBW: 1 MHz, span: 50 MHz

We plot a heatmap of the measured  $f_{rep}$  signal in Fig. 8 to show behavior of the  $f_{rep}$  signal in PML and SIL regimes when the VOD is varied. Varying the optical delay moves the fiber modes within the passband of the FPE. From the plot it can be observed that highest supermode suppression occurs at a delay of 40 - 50 ps, indicating optimal overlap of the fiber feedback modes within the passband of the FPE.

## IV. COUPLED OPTO-ELECTRONIC LOOP AND REFERENCING

In this section we will discuss the implementation of a coupled optoelectronic loop (COEL) with the MLL under self-injection locking operation with filtered feedback as depicted in Fig. 9. Output from the injection locked MLL is passed through an isolator and a coupler which goes to the diagnostics and a photodetector. The photodetected signal is amplified with an RF amplifier and sent through a 10 dB directional coupler

Fig. 9. Schematic of the monolithic InP MLL, optical filtering, injection locking and coupled opto-electronic loop (COEL) apparatus used in the experiment. EAM: Electro-absorption modulator, MMI: Multi-mode interference coupler, SOA: Semiconductor optical amplifier, SA: Saturable absorber, FPE: Fabry-Perot etalon, VOD: Variable optical delay, VOA: Variable optical attenuator, ISO: Isolator, Amp: RF amplifier, Syn: RF synthesizer, mixer: high frequency mixer, LPF: Low pass filter, PS: tunable RF phase shifter, P-I: Servo controller, OSA: Optical spectrum analyzer, RFSA: RF spectrum analyzer, FC: Frequency counter

to split the signal for diagnostics and the COEL. The output from the directional coupler is amplified to 10 dBm with an RF amplifier and sent through a 3dB directional coupler, where one port goes to the voltage controlled RF phase-shifter (Micronetics CPS-4036) and the other port goes to the RF port of the high frequency mixer. A 10 GHz RF synthesizer (Agilent 8988) is used as the local oscillator input to the high frequency mixer. The output mixed signal from the IF port of the mixer is passed through a low pass filter (LPF) and sent to the PID servo controller that provides the control voltage to the tunable RF phase-shifter. Output from the RF phase shifter is then used to drive the integrated EAM. The applied RF power at the integrated EAM is  $\sim 0~{\rm dBm}$ .

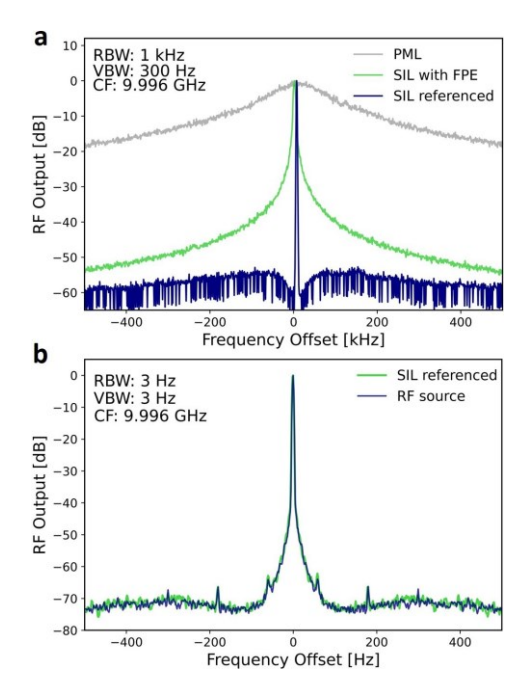


Fig. 10. (a) RF spectrum of the photodetected  $f_{rep}$  signal with the MLL under PML, SIL with FPE and SIL with FPE with the COEL referenced to an external RF source (SIL referenced), CF: center frequency (b) RF spectrum of the source and measured  $f_{rep}$  signal of the MLL under SIL referenced operation

Fig. 10a shows the photodetected  $f_{rep}$  signal of the MLL under PML, SIL with FPE and SIL with FPE with the COEL referenced to an external RF source (SIL referenced). The plot shows a significant phase noise reduction when the COEL is locked to the RF source. At 100 kHz offset from the carrier, the RF spectrum of the measured  $f_{rep}$  signal shows > 15 dB noise suppression in comparison to the MLL under SIL with FPE operation and > 45 dB in comparison to the MLL under PML operation. The dip in the noise floor closer to the carrier in the case of SIL referenced operation is due to the locking bandwidth of the servo controller. The RF spectrum of the source and the  $f_{rep}$  signal of the MLL under SIL referenced operation is shown in Fig. 10b. The  $f_{rep}$  signal of the MLL closely follows the RF source confirming a good lock with the source, improving the noise performance as expected.

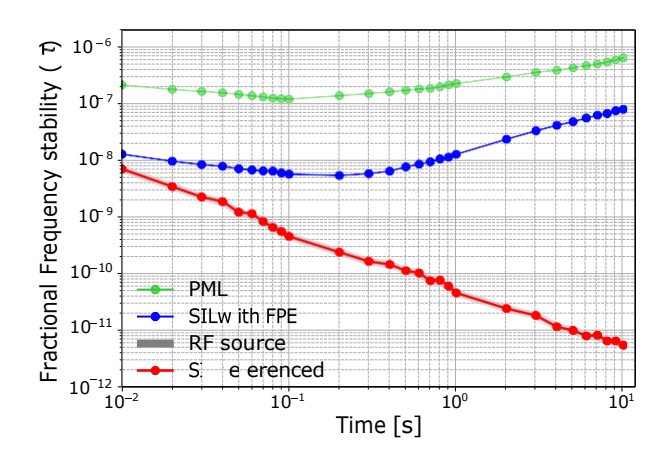


Fig. 11. Measured fractional frequency stability (ADEV) of the photodetected  $f_{rep}$  signal when the MLL is operating under PML, SIL with FPE and SIL referenced to the external RF source

The optical linewidth, optical spectrum and pulse intensity autocorrelation of the MLL under SIL referenced operation does not show any deviation from the MLL under SIL with FPE operation. Finally, we used a zero dead time frequency counter (Pendulum 4545) to measure the fractional frequency stability of the  $f_{rep}$  signal of the MLL under PML, SIL

with FPE and SIL referenced operation. Using this frequency counter data, we computed the Allan deviation (ADEV) and plotted in Fig. 11. For the MLL under PML operation the calculated ADEV from the measured fractional frequency stability is  $2.2 \times 10^{-7}$  at 1s averaging time and  $7 \times 10^{-7}$  at 10 s averaging time. Under SIL with FPE operation the ADEV at 1s averaging time is  $\sim 1 \times 10^{-8}$ , which is an order of magnitude improvement over PML operation. When the laser is under SIL referenced operation, the ADEV of the MLL follows that of the RF source, indicating the stability transfer from the RF source to the MLL. The ADEV at 10 s averaging time is  $5 \times 10^{-12}$  which is an improvement of 5 orders of magnitude over PML operation.

#### V. CONCLUSION AND OUTLOOK

In this work, we presented a self-injection locking technique to improve the stability and noise performance of an integrated semiconductor mode-locked laser, using a Fabry-Perot Etalon as the photonic filter. This technique is implemented by passing the PML laser output through the FPE, whose airy peak width is less than the optical axial linewidth of the MLL. The FPE is placed in a fiber feedback loop that injects the filtered signal from the FPE back into the MLL to enable self-injection locking. When the MLL is under SIL with FPE operation, the RF linewidth of the frep signal narrowed by a factor of 50, from 109 kHz (FWHM) to 2.2 kHz (FWHM). In addition, the supermodes from the fiber feedback path are suppressed by 20 dB, due to filtering effect of the FPE. The optical axial mode linewidth is reduced by a factor of 100, from 600 MHz (FWHM) for PML operation to 6 MHz (FWHM) for SIL with FPE operation. With the MLL under SIL with FPE operation, the Allan deviation of the free signal shows a magnitude of improvement over the PML operation at 1s averaging time. Finally, we implemented a COEL with the photodetected signal from the MLL under SIL with FPE operation and referenced the system to an external RF source by driving the integrated EAM in the MLL cavity. Measured RF spectrum of the  $f_{rep}$  signal shows a significant improvement in phase noise and stability, showing how well the system inherits the properties of the reference RF source. The RF phase noise at 100 kHz offset from the carrier is improved by > 15 dB compared to the SIL with FPE operation and > 45 dB compared to the free-running PML operation. The Allan deviation at 10 s averaging time is  $5 \times 10^{-12}$ , showing an improvement of 5 orders of magnitude over PML operation.

Future improvements of this technique could be done using a miniaturized FPE [22] or WGMR [23] with narrower passband to improve the filtering effects and compactness. Further optimization of the MLL cavity can be done using III-V on silicon approach, where InP gain and saturable absorber sections are deposited on silicon and utilize low-loss silicon waveguide for the rest of the cavity [24]. The III-V on silicon approach also offers potential for integrating long high-Q low-loss silicon spiral waveguides that can be used as a filter cavity coupled to the MLL [25]. These future steps towards integration and utilizing miniaturized components could enable the current tabletop system to achieve SWaP benefits, while

offering narrow linewidth and low-noise performance mode-locked lasers.

#### REFERENCES

- [1] M. U. Piracha *et al.*, "Simultaneous ranging and velocimetry of fast moving targets using oppositely chirped pulses from a mode-locked laser," *Optics express*, vol. 19, no. 12, pp. 11 213–11 219, 2011.
- [2] K. Y. Yang et al., "Multi-dimensional data transmission using inversedesigned silicon photonics and microcombs," vol. 13, no. 1, p. 7862, 2022.
- [3] T. Fortier et al., "20 years of developments in optical frequency comb technology and applications," Communications Physics, vol. 2, 12 2019.
- [4] P. J. Delfyett et al., "Optical frequency combs from semiconductor lasers and applications in ultrawideband signal processing and communications," *Journal of Lightwave Technology*, vol. 24, no. 7, p. 2701, 2006.
- [5] G.-H. Duan et al., "High performance inp-based quantum dash semiconductor mode-locked lasers for optical communications," Bell Labs Technical Journal, vol. 14, no. 3, pp. 63–84, 2009.
- [6] R. Bustos-Ramirez et al., "Synchronization of electro-optically modulated kerr soliton to a chip-scale mode-locked laser pic via regenerative harmonic injection locking," Journal of Lightwave Technology, vol. 40, pp. 1742–1748, 3 2022.
- [7] S. V. Pericherla et al., "External cavity optical filtering and self-injection locking a chip-scale mode-locked laser using a fabry-perot etalon," in 2023 IEEE Photonics Conference (IPC), 2023, pp. 1–2.
- [8] S. Liu et al., "High-channel-count 20 ghz passively mode-locked quantum dot laser directly grown on si with 4.1 tbit/s transmission capacity," Optica, vol. 6, no. 2, pp. 128–134, 2019.
- [9] V. Moskalenko et al., "Record bandwidth and sub-picosecond pulses from a monolithically integrated mode-locked quantum well ring laser," Optics Express, vol. 22, no. 23, pp. 28 865–28 874, 2014.
- [10] H. Asghar et al., "Optimum stabilization of self-mode-locked quantum dash lasers using dual optical feedback with improved tolerance against phase delay mismatch," Optics Express, vol. 25, p. 15796, 7 2017.
- [11] R. B. Ramirez *et al.*, "Regenerative multi-tone injection locking for linewidth enhancement and repetition rate stabilization of a pic mode-locked laser," pp. 195–196, 2017.
- [12] C. Henry, "Theory of the linewidth of semiconductor lasers," *IEEE Journal of Quantum Electronics*, vol. 18, no. 2, pp. 259–264, 1982.
- [13] J. van der Ziel, "Spectral broadening of pulsating al x ga 1-x as double heterostructure lasers," *IEEE Journal of Quantum Electronics*, vol. 15, no. 11, pp. 1277–1281, 1979.
- [14] G. Liu et al., "Measurement of linewidth enhancement factor of semiconductor lasers using an injection-locking technique," *IEEE Photonics Technology Letters*, vol. 13, no. 5, pp. 430–432, 2001.
- [15] Y. Takushima et al., "Linewidth of mode combs of passively and actively mode-locked semiconductor laser diodes," vol. 5595, pp. 213–227, 2004.
- [16] R. Galiev et al., "Spectrum collapse, narrow linewidth, and bogatov effect in diode lasers locked to high-q optical microresonators," Optics express, vol. 26, no. 23, pp. 30 509–30 522, 2018.
- [17] L. Hao et al., "Narrow-linewidth self-injection locked diode laser with a high-q fiber fabry-perot resonator," Optics Letters, vol. 46, no. 6, pp. 1397–1400, 2021.
- [18] A. Bhardwaj et al., "A monolithically integrated racetrack collidingpulse mode-locked laser with pulse-picking modulator," *IEEE Journal* of Quantum Electronics, vol. 56, 8 2020.
- [19] T. Habruseva et al., "Optical linewidth of a passively mode-locked semiconductor laser," Optics letters, vol. 34, no. 21, pp. 3307–3309, 2009.
- [20] G. Liu et al., "Measurement of linewidth enhancement factor of semiconductor lasers using an injection-locking technique," *IEEE Photonics Technology Letters*, vol. 13, no. 5, pp. 430–432, 2001.
- [21] P. Laurent et al., "Frequency noise analysis of optically self-locked diode lasers," *IEEE Journal of Quantum Electronics*, vol. 25, no. 6, pp. 1131– 1142, 1989.
- [22] C. A. McLemore, N. Jin, M. L. Kelleher, J. P. Hendrie, D. Mason, Y. Luo, D. Lee, P. Rakich, S. A. Diddams, and F. Quinlan, "Miniaturizing ultrastable electromagnetic oscillators: Sub-10- 14 frequency instability from a centimeter-scale fabry-pe'rot cavity," *Physical Review Applied*, vol. 18, no. 5, p. 054054, 2022.
- [23] V. S. Ilchenko et al., "Crystal quartz optical whispering-gallery resonators," Optics letters, vol. 33, no. 14, pp. 1569–1571, 2008.
- [24] Z. Wang et al., "A iii-v-on-si ultra-dense comb laser," Light: Science and Applications, vol. 6, 2017.
- [25] J. Guo et al., "Chip-based laser with 1-hertz integrated linewidth," Sci. Adv, vol. 8, p. 9006, 2022. [Online]. Available: https://www.science.org